PCCP

PAPER

View Article Online
View Journal | View Issue

Cite this: *Phys. Chem. Chem. Phys.*, 2017, **19**, 10854

Influence of orientation mismatch on charge transport across grain boundaries in tri-isopropylsilylethynyl (TIPS) pentacene thin films†

Florian Steiner,‡[a] Carl Poelking,‡[b] Dorota Niedzialek,[a] Denis Andrienko[b] and Jenny Nelson*[a]

Received 19th September 2016,
Accepted 14th February 2017

DOI: 10.1039/c6cp06436a

rsc.li/pccp

We present a multi-scale model for charge transport across grain boundaries in molecular electronic materials that incorporates packing disorder, electrostatic and polarisation effects. We choose quasi two-dimensional films of tri-isopropylsilylethynyl pentacene (TIPS-P) as a model system representative of technologically relevant crystalline organic semiconductors. We use atomistic molecular dynamics, with a force-field specific for TIPS-P, to generate and equilibrate polycrystalline two-dimensional thin films. The energy landscape is obtained by calculating contributions from electrostatic interactions and polarization. The variation in these contributions leads to energetic barriers between grains. Subsequently, charge transport is simulated using a kinetic Monte-Carlo algorithm. Two-grain systems with varied mutual orientation are studied. We find relatively little effect of long grain boundaries due to the presence of low impedance pathways. However, effects could be more pronounced for systems with limited inter-grain contact areas. Furthermore, we present a lattice model to generalize the model for small molecular systems. In the general case, depending on molecular architecture and packing, grain boundaries can result in interfacial energy barriers, traps or a combination of both with qualitatively different effects on charge transport.

1 Introduction

Solution-processing of small-molecule crystallisable semiconductor films generally leads to polycrystalline films containing crystallites with sizes of tens of nm to several μm separated by grain boundaries and amorphous interphases.[1–4] The presence of grain boundaries reduces charge carrier mobilities compared to single-crystal films, deteriorating device characteristics such as the switching speed of field-effect transistors (FET). Although much effort has been spent on increasing crystal sizes,[5–8] this strategy does not always succeed, since even a few grain boundaries can be sufficient to impede device performance severely.[9–12]

Several studies have addressed the impact of grain boundaries on hole mobilities in thin molecular films, usually in FET structures, with particular attention paid to pentacene derivatives and similar materials. Within single-crystal grains, charge-carrier mobilities can be highly orientation dependent with mobility anisotropies larger than 10.[13,14] Kelvin probe force microscopy studies of pentacene thin films indicate surface potential wells at grain boundaries, suggesting trap states for electrons.[15] This observation is in agreement with conductive probe atomic force microscopy results revealing several orders of magnitude higher resistances at grain boundaries than within grains.[1] Rivnay and co-workers suggested that the impact of grain boundaries on charge transport is dependent on the crystal packing structure.[11] Their qualitative picture implied that herringbone packed materials (*e.g.* pentacene) suffer less from grain boundaries than materials in brickwork structures (*e.g.* TIPS-P). The larger the mutual angle between grains, the more severe would be the effect of grain boundaries due to reduced electronic coupling of molecules at the interface. Such an angular dependence is supported by a study by Lee *et al.* obtaining lower mobilities for larger mutual angles between grains for 5,11-bis(triethylsilylethynyl)anthradithiophene (TES-ADT).[16] In the studies of Lee *et al.* and Rivnay *et al.*, the general picture is that grain boundaries in small molecular systems are sharp and abrupt. In contrast, Wong and co-workers claim that grain boundaries between TIPS-P grains consist of small crystals that are connected to each other, and that contact regions between grains should be small and separated by voids.[17] Until now, there is limited information about molecular packing patterns close to grain boundaries.

[a] *Department of Physics and Centre for Plastic Electronics, Imperial College London, London SW7 2AZ, UK. E-mail: jenny.nelson@imperial.ac.uk*
[b] *Max Planck Institute for Polymer Research, Ackermannweg 10, 55128 Mainz, Germany*

† Electronic supplementary information (ESI) available. See DOI: 10.1039/c6cp06436a
‡ These authors contributed equally to this work.

A numerical model of the impact of grain boundaries on charge transport in organic semiconductor films would be helpful in quantifying the effect on devices. Most prior work has addressed phenomena in inorganic semiconductors. Kelvin probe measurements of the surface potential on polycrystalline silicon have led to drift-diffusion models with trap states at the grain interface.[18,19] The method was later adapted for other polycrystalline inorganic and organic semiconductors.[20,21] The approach suggests that in organic FETs high charge concentrations in the channel lead to back-to-back Schottky barriers forming around grain boundaries. Despite allowing for an effective-medium interpretation of device characteristics, these drift-diffusion-based models are restricted to one dimension using fitted macroscopic parameters (*e.g.* trap concentration, width of grain boundaries). Moreover, the formation of back-to-back Schottky barriers requires high doping concentrations at the grain boundary which is unlikely for organic semiconductors. Whilst few previous studies have addressed the energetic profile around grain boundaries in organic semiconductors, donor–acceptor interfaces have been studied on a molecular scale to understand exciton dissociation in organic solar cells.[22–25] Cornil and co-workers could show that the energy landscape at the interface between two different materials depends on the mutual orientation of the molecules.[22] Moreover, Poelking *et al.* suggested that long-range interactions are crucial to understand level alignment at donor–acceptor interfaces.[24,25] The effect of grain boundaries on mobility in organic thin films was simulated for a range of molecular structures by Park and co-workers using a multi-scale approach, resulting in a clear dependence of mobility on grain size.[26] However, this study stopped short of any atomistic treatment of structure and dynamics at the grain boundary. Using a different approach, Mladenovic investigated grain boundaries of polycrystalline naphthalene simulated with a Monte-Carlo method assuming Van-der-Waals interactions between rigid naphthalene segments. Charge densities and single-particle potentials are calculated with a charge patching method. The authors find deeper traps for low-angle grain boundaries.[27] These previous studies leave a number of open questions that need to be treated at a molecular level, namely: (1) how grain boundaries affect the energetic profile for charge carriers and hence charge transport, and (2) how the relative orientation of grains affects charge transport.

In this study, we use multi-scale simulation to address the impact of grain boundaries on the energy landscape and on the strength of electronic coupling across the grain boundary. Charge transport in FETs can be considered quasi two-dimensional along a channel parallel to the gate electrode.[28] We use atomistic molecular dynamics to simulate molecular packing around grain boundaries in two-dimensional structures with varied angle ϑ between the grain orientations, and use a kinetic Monte-Carlo hopping model to explore the dependence on ϑ of the rate of hole transport across grains. The energetic landscape across the grain boundary is modelled by calculating electrostatic and inductive contributions to site energies. We find that the grain boundary in TIPS-P introduces a barrier to charge transport, but that the impact on transport across the boundary is weak and almost independent of ϑ, unless the contact area between grains is small. Extensions to the approach using a lattice description show that in general grain boundaries may lead to interfacial energetic barriers, energetic traps, or both, depending on the molecular architecture, packing and the charge-carrier type (electron or hole).

2 Modelling methods

We use a combination of methods to generate molecular assemblies, calculate site energies and simulate charge transport as detailed in the following paragraphs.

(i) Generating molecular assemblies containing grain boundaries

Generating realistic molecular assemblies of relevant size for charge transport simulations is challenging due to computational constraints.[29] In this case the challenge is simplified first by the fact that charge transport in FETs is confined to a thin (here approximated with a 2D) channel and second by the tendency of TIPS-P to organise with the *a*–*b* plane parallel to the substrate (*e.g.* on silicon, glass and amorphous carbon[30]). In this plane, TIPS-P exhibits good two-dimensional transport properties due to high transfer integrals in the *a* and *a*–*b* directions, constraining charge transport to a more or less two-dimensional plane since coupling in the *c* direction is very weak.[31] In this study we take two approaches to generate representative systems. First, we use atomistic molecular dynamics (MD) to simulate the arrangement of TIPS molecules around grain boundaries in a two-crystallite system. For more general studies of the nature of grain boundaries we generate multi-grain structures with abrupt interfaces by simulating growth of ordered domains around randomly oriented seeds. Each lattice site is populated with an anisotropic quadrupolar particle.

To generate polycrystalline assemblies, we first prepare two crystalline grains with a mutual orientation ϑ (the relative orientation of corresponding **a** vectors, the grain interface is parallel to the **a** vector). ϑ is varied between 0 (parallel grains) and 90° (vertical grains) in steps of 22.5°. Initially, both grains are built using the crystal structure of ref. 32. The first grain is interrupted along an edge parallel to the **a**-vector, and the second grain is continued until the closest atoms of the two grains are separated by less than 1 nm. This distance is close enough for TIPS-P molecules of different grains to interact, and far enough to allow for orientational and positional relaxation at the grain-interface during the MD simulation. We developed a force-field specific to TIPS-P, starting with the OPLS reference data base.[33] Force-field parameters between silicon atoms (in the TIPS-P side-chains) and surrounding bonded sp^3-hybridised carbon atoms are taken from Guilbert *et al.*[34] and those between the silicon and the bonded sp-hybridised carbon are fitted by comparing molecular mechanics calculations with a molecular structure derived from hybrid density functional theory calculations (B3LYP/6-311g(d,p)). The fitting process of force-field parameters was repeated iteratively until bond length differences between the optimised quantum-chemical geometry and the structure

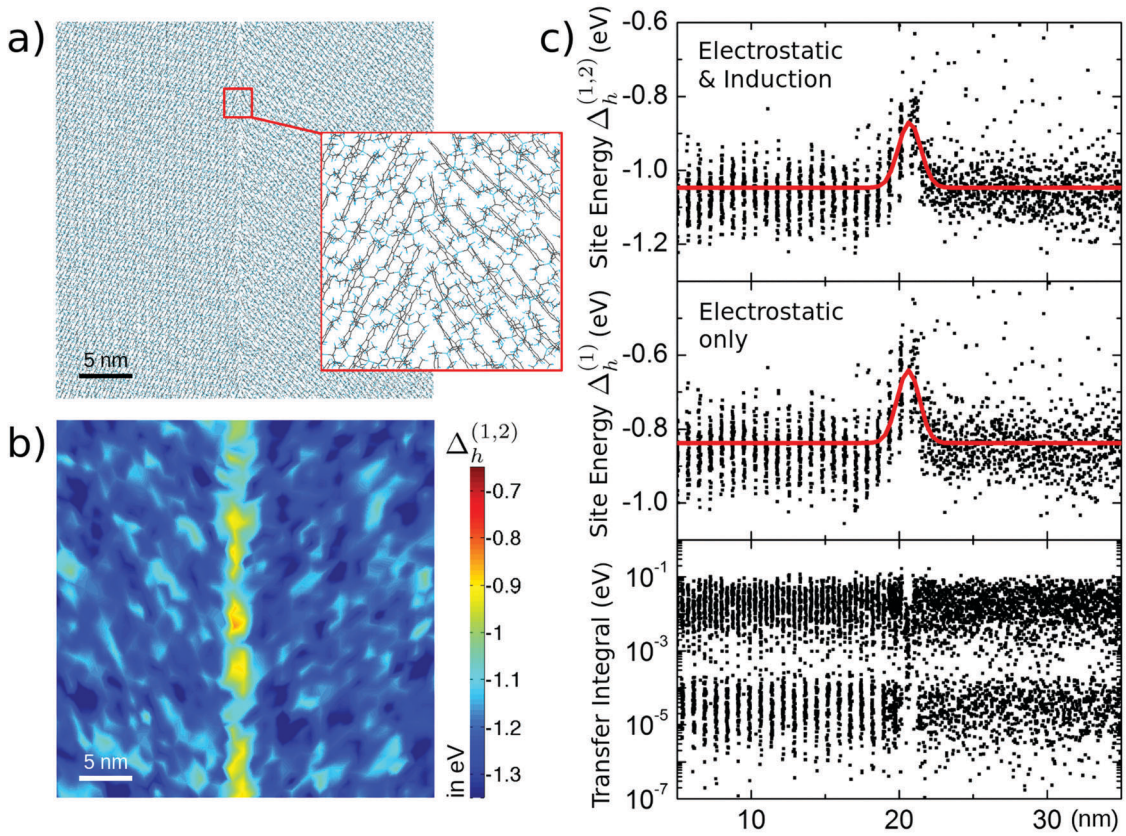

Fig. 1 Results of molecular dynamics simulations and computation of site energies and transfer integrals for a mutual angle ϑ of 67°. (a) Equilibrated molecular dynamics structure after 10 ns, (b) energy landscape for cutoff calculations including electrostatics and polarization for the structure shown in (a) and (c) projection of site energies (top) and (middle) and transfer integrals (bottom) onto the axis perpendicular to the grain boundary. Holes are stabilised at more negative energies, and less negative energies represent a barrier for holes.

calculated with molecular mechanics were below 0.001 Å. The complete force-field for TIPS-P can be found in ESI,† Section A.

The initial, two-crystalline grain structures are relaxed in an *NPT* ensemble using the developed force field. Pressure is applied with an anisotropic barostat (Berendsen) parallel to the two-dimensional system. The equilibration is performed under periodic boundary conditions. Note that the out-of-plane cell dimension of the 2D system is 5 nm, preventing interactions along this direction. MD simulations are run for 10 ns. The resulting molecular assemblies are rectangular with side-lengths of about 40 nm and contain around 2600 molecules. Fig. 1a illustrates an equilibrated structure with a mutual angle ϑ of 67.5°. Grains maintain their general alignment during equilibration, *i.e.*, the grain orientation is still visible in the final structures. Exclusively at the interface between grains, molecules displace and can adopt completely different orientations. Parallel grains ($\vartheta = 0°$) fuse together and hence no grain boundary is observable after relaxation. For the charge transport calculations, snapshots are extracted after 6, 7, 8, 9, and 10 ns for each configuration angle ϑ.

For studies of multigrain systems we use a version of this approach where rather than starting with two crystalline grains and a simple linear interface we start with a number of crystalline grains seeded at random position and random orientation in the simulation plane. The grains are allowed to grow through the random attachment of individual molecules, preserving the crystal structure of the growing grains. Growth continues until molecules within different grains come within 1 nm of each other, resulting in several, uneven grain boundaries. The structures are equilibrated with the same force field as for the two grain structures. We refer to this process as 'probabilistic growth'. Further details are given in the ESI,† Section G.

To generate structures for the lattice model calculations, several (approximately) periodically matched sublattices assembled from unit cells with varying orientations are superimposed and seeded independently, where each sublattice corresponds to a given in-plane crystallite alignment. The unit cell of the crystals has a face-centred square structure (lattice constant $c = 0.7$ nm) with a monomolecular basis of quadrupole moment ($Q_{20} = -10$ a.u.) lattice sites. The individual grains are subsequently grown probabilistically until the simulation cell of $75 \times 75 \times 5$ nm^3 is densely populated based on a site–site exclusion potential $V(i,j) = \infty$ if $r_{ij} \leq r_c$, else 0, with particle indices i,j and cutoff $r_c = \sqrt{3}/2c$.

(ii) Site-energy calculations

Site energies E are computed either by considering only electrostatic interactions or considering both electrostatic and

polarization interactions following ref. 35. Molecular fields are parametrized *via* a distributed multipole analysis built on atomic expansion sites. The molecular field response is described within the Thole point-dipole model, which damps dipole–dipole interactions at short distances to correct for unphysical polarization divergences. The established way of calculating site energies from electrostatics and polarization is by assuming an interaction cutoff, beyond which no interactions between multipoles are considered, to reduce computational effort. For comparison, we also include a long-range polarized embedding technique which rigorously accounts for long-range interactions.[24,25] Within the lattice model, the same approach is applied, using a single-site electrostatic representation of the molecular building blocks.

(iii) Transport simulation

Charge transport is simulated for two-grain MD-generated structures with a kinetic Monte-Carlo approach using a home-built code (ToFeT[36]) based on a hopping model of transport where charges are instantaneously localised on a single molecule. In TIPS-P, a hopping picture may be considered of marginal validity since prior measurements revealed a Hall effect[37] which is indicative of a more extended transport mechanism. However, in a heterogeneous system containing grain boundaries and disordered regions, as studied here, transport will be rate limited by hopping events between weakly coupled sites. For this reason, as well as for the practical expediency of simulating usefully large systems, we use the hopping picture. Hopping rates are computed from non-adiabatic Marcus theory.[38] An electric field of 10^7 V m^{-1} is applied perpendicularly to the grain boundary, corresponding to the field-independent regime of the charge-carrier mobility. Hole mobilities are quantified by the average time taken to cross the entire two-grain ensemble under the given electric field. Simulations are run in the limit of low carrier concentrations and charges are launched and collected in contact regions of width 2 nm at each end. The hopping rate requires values for the hole coupling, J reorganisation energy, λ and the difference in energy between initial and final sites. Previously, we calculated the inner-sphere reorganisation energy of TIPS-P to be 138 meV.[31] The external contribution to the reorganisation energy must be added to this inner-sphere contribution, but is hard to estimate.[39] The absence of thermal activation in the experimental hole mobility of TIPS-P[40] indicates that a high overall reorganisation energy would not be appropriate. For this reason we choose a low value of the outer reorganisation energy for TIPS-P of $\sim$60 meV, to yield a total value for λ of 200 meV. We note that this value of λ is large compared to the values of hole transfer integrals in equilibrated structures at room temperature (shown in Fig. 1(c) below) and is consistent with the use of a hopping model at room temperature. However, at low temperature, reduced thermally induced disorder in site energy and coupling is likely to lead to more extended charge states and make the hopping model less appropriate. For completeness, we also considered λ = 0.5 eV and found the same relative effects of grain boundaries on hole transport. We note that, provided that the outer reorganisation energy is not strongly affected by the grain boundaries, (justified below for the present case) the effect of changing λ is primarily to change the magnitude of the room-temperature mobility but not the trend.

Charge-transfer integrals J are computed with the Molecular Orbital Overlap (MOO) method.[41] MOO allows fast evaluation of electronic coupling elements compared to other approaches such as the projective method,[42] since orbitals are calculated with the semi-empirical differential overlap functional ZINDO and complete electronic structure calculation of molecular pairs can be omitted. MOO has previously been tested in comparison with projective and other methods by us[43,44] and others.[45] The increased computation speed is of great advantage for systems with several thousand molecules as in this study. The ZINDO parametrization excludes heavy elements such as silicon. Therefore, we drop parts of the side-chain structure of TIPS-P for transfer integral calculations by substituting the isopropylsilyl-group with a hydrogen atom (see ESI,† Section B). We believe that this is a good approximation for transfer integral calculations given that the π-electron system of TIPS-P is located on the pentacene core and not on the silyl end groups. ESI,† Section B illustrates that transfer integrals from the projective method (full TIPS-P geometry) and MOO (reduced geometry with hydrogen instead of silicon) are very similar and the two-dimensional transport behaviour is preserved. Considering the ideal crystal structure of TIPS-P in ref. 32, the two dominant coupling elements in the a and a–b direction amount to 85.7 meV and 70.0 meV, respectively, when calculated with MOO indicating strong and fairly isotropic coupling. We note that the highest J values are not small compared to the value of λ used, and in such a regime non-adiabatic Marcus theory may be inappropriate. However, as we show below, the values of J are greatly reduced by disorder and at grain boundaries making the hopping picture appropriate for these rate limiting events. A useful account of the applicability of Marcus theory is provided by Spencer *et al.*[46]

3 Results and discussion

Effect of grain boundaries on charge transport in atomistic structures

At first we study how grain boundaries influence charge transfer parameters. Fig. 1 summarises the findings for a two-grain structure generated using atomistic MD with a mutual angle ϑ of 67.5°. Apart from the case of ϑ = 0°, all structures show visible disruption at the grain boundary and elevated hole site energies for the molecules lying between the grains. Generally, the barrier created by these deeper hole sites tends to be non-uniform (see Fig. 1b). Peak barrier heights tend to increase with ϑ (see ESI,† Section D). The first two graphs of Fig. 1c show site energy as a function of position along the normal to the grain boundary. Compared to electrostatics-only calculations, polarization slightly reduces energetic disorder and homogeneously stabilizes energy levels by around 0.2 eV. The effect of polarization is relatively small due to the membrane-like, rather than bulk-like, setup. The average energy barrier height is, however, maintained.

The bottom graph in Fig. 1c shows transfer integrals as a function of position along the normal to the grain boundary. Each transfer integral is assigned to the center of mass position of the charge-transfer pair. Within the grains, two bands at around 10^{-2} meV and 10^{-5} meV can be observed. The former relates to the strong electronic coupling along the *a* and *a–b* directions, whereas the latter reflects transfer along the *b* direction (for which J = 0.21 meV in the crystal). The *a* and *a–b* transfer integrals are slightly smaller than in the ideal crystal structure of TIPS-P due to structural disorder introduced by molecular dynamics. At the grain boundary, the bands are interrupted and the highest transfer integrals are reduced by an order of magnitude. The higher the mutual angle ϑ, the larger is the reduction in electronic coupling at the grain boundary (see ESI,† Section E)

The results of our microscopic calculations are in line with the experimental observation, using Kelvin probe, of a potential well for electrons in pentacene. At grain boundaries we observe barriers for hole transport, but since electrons and holes see opposite energy landscapes and Kelvin probe measures the electron's energy landscape, energy barriers for hole transport would appear as potential wells in Kelvin probe measurements. Simulated and experimental potential well depths are both on the order of 100 meV.[15] Moreover, we find that the inter-granular trap depth is non-uniform. Similar to the picture developed by Rivnay *et al.*,[11] the electronic coupling decreases with increasing mutual angles ϑ.

To study the effect of these barriers on hole mobility, we simulated hole transport on two types of structure, (i) the complete 400 × 400 Å^2 atomistic MD structures representing long grain boundaries and (ii) narrower 40 × 400 Å^2 stripes intended to represent limited contact length between grains. Fig. 2 summarises the results for the complete 400 × 400 Å^2 molecular assemblies. Mobilities are simulated both with the energetic disorder that results from electrostatic and polarisation interactions (we refer to the mobilities calculated in this case with the symbol μ) and without energetic disorder (for which we use the symbol $\mu_{E=\text{const}}$). Furthermore, mobilities of the ideal crystal structure of TIPS-P (indicated by μ_{Xtal}) are calculated through direct solution of the Master equation, as done previously in ref. 31. Here, μ_{Xtal} excludes disorder in both site energies and electronic couplings, such that this mobility depends solely on the crystal orientation of the two grains[31] and is dominated by the lower of the two mobilities. As described above, we consider for each angle ϑ 5 different molecular assemblies (molecular dynamics snapshots) separated by 1 ns in time. Mobility ratios are calculated individually for each structure. Subsequently, the average ratio is computed. For reference, the absolute value of μ computed for a single crystal is in the range 3 to 10 cm^2 V^{-1} s^{-1}, depending on direction within the *ab* plane.

Fig. 2, top panel, reflects the influence of the energy landscape on hole mobilities, which is approximately constant for all angles. For each ϑ, electrostatics-only calculations exhibit on average lower mobilities than simulations including polarization. This may be attributed to the decrease in energetic disorder upon polarization (see the previous section). Comparing mobilities at

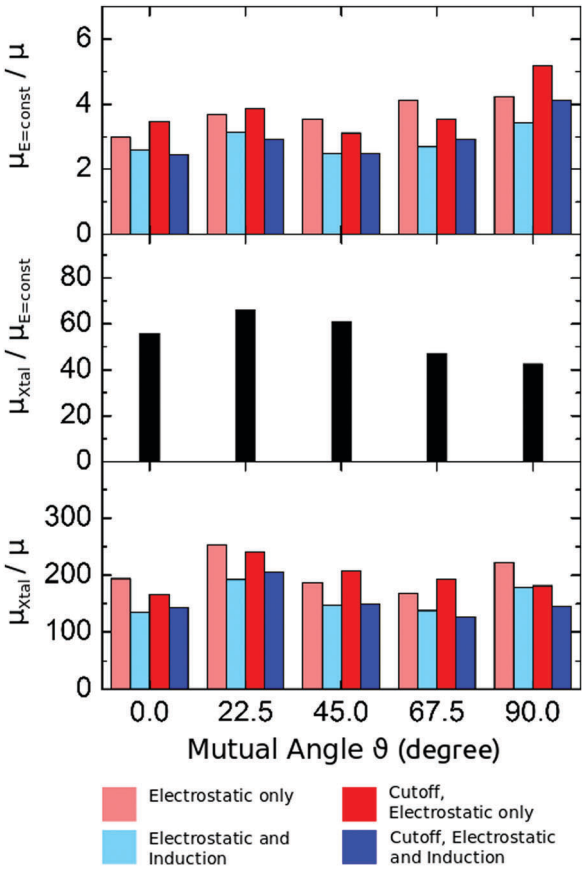

Fig. 2 Results of charge transport simulations of large, 400 × 400 Å^2 structures with one grain boundary and varied mutual crystal orientations. μ_{Xtal} is defined as the average of the reciprocals of mobility along the normal to the grain boundary for the two ideal crystal grains, $\mu_{E=\text{const}}$ relates to the mobility of the equilibrated molecular dynamics structure without energetic disorder and μ is the mobility of the equilibrated molecular dynamics structure including energetic disorder. The mobility ratios quantify the effect of grain boundary on charge transport and are averages over 5 structures per angle. Top, effect of the energy landscape; middle, effect of disorder in electronic coupling; and bottom, total mobility reduction factor due to grain boundary.

constant site energies and in the ideal crystal structure allows an estimation of the effect of disorder in electronic couplings (see Fig. 2, middle panel). Just as for the energy landscape, there is no obvious ϑ-dependence of the effect of disorder in electronic couplings on charge transport. Disorder in transfer integrals, however, seems to have a stronger effect on the magnitude of mobilities than disorder in site energies: the average ratio $\mu_{E=\text{const}}/\mu$ is around 4, whereas $\mu_{\text{Xtal}}/\mu_{E=\text{const}}$ exceeds 50. Also shown in Fig. 2 are cutoff calculations at 8 nm and the results are similar. This indicates that the energy distortion at the grain interface is dominated by short range interactions.

Finally, the mobility reduction compared to the ideal crystal structure without disorder in electronic couplings and site energies is presented in Fig. 2, bottom panel. For 0°, the average mobility ratio μ_{Xtal}/μ is slightly lower than for larger ϑ. Again, no clear trend for increasing ϑ is observable. Thus, whilst these results support the observation of reduced mobility in the presence of grain boundaries, the large, 400 × 400 Å^2

morphologies appear unable to explain the experimentally observed grain angle dependence of the mobility reductions.[9,11] As we, however, discussed in the previous section, barrier height and transfer integrals are non-uniform at the grain/grain interface. We will show below that charge carriers are as a result likely to find 'sweet spots' along the boundary, characterized by a smaller energy barriers and strong electronic couplings, for all mutual orientations.

The way the situation changes when confining charge transport to 40 Å wide boundary stripes is summarized in Fig. 3. Here, we consider 4 stripes for each of the 5 molecular assemblies per angle ϑ with ranges $x_0 - x_1$ = 12–16 nm, 16–20 nm, 20–24 nm, 24–28 nm, where x is the axis parallel to the grain boundary, and find the mobility for each situation. Since the origin of the energy barrier at the grain/grain interface is due to short-range interactions, we consider in the following only site energies from cutoff calculations. Compared to transport simulations on full, 400 Å wide molecular structures, the variance of modelled mobilities is increased. If we consider the ratio μ_{Xtal}/μ, the average of this ratio is larger due to the greater variance than in the case of long boundaries (see Fig. 3 and ESI,† Section F).

The influence of the energy surface increases towards larger ϑ, resulting in an average mobility ratio of over 20 for $\vartheta = 90^\circ$. The restriction to short boundaries results in an intergranular interface that is normally too short for charge carriers to find a low-energy region of the boundary. As before, calculations including polarization result in higher mobilities compared to electrostatics-only simulations. $\mu_{\mathrm{Xtal}}/\mu_{E=\mathrm{const}}$ generally increases with ϑ although the trend shows some variation, assigned to high variances of modelled mobilities when considering 40 Å wide stripes (see ESI,† Section F). Finally, the ratio between simulated mobilities with disorder in site energies and electronic couplings *versus* the mobility of ideal crystal structures increases with ϑ. For 90°, the average mobility ratio μ_{Xtal}/μ is more than five times higher than for 0°.

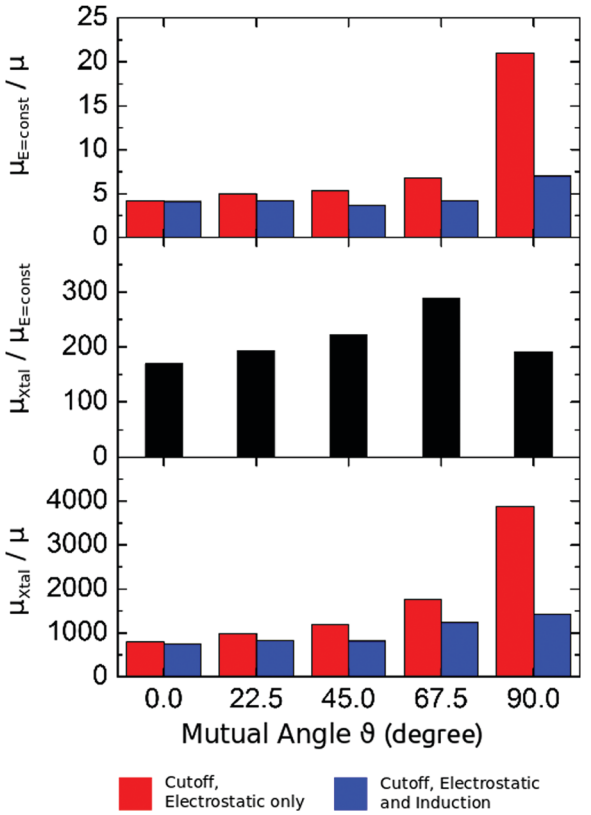

Fig. 3 Results of charge transport simulations of small, 40 × 400 Å^2 structures with one grain boundary and varied mutual crystal orientations. μ_{Xtal} is defined as the reciprocal of the average of the reciprocals of mobility along the normal to the grain boundary for the two ideal crystal grains, $\mu_{E=\mathrm{const}}$ relates to the mobility of the equilibrated molecular dynamics structure without energetic disorder and μ is the mobility of the equilibrated molecular dynamics structure including energetic disorder. The mobility ratios quantify the effect of grain boundary on charge transport and are averages over 20 structures per angle and depict: top, effect of the energy landscape: middle, effect of disorder in electronic coupling; and bottom, total mobility reduction factor due to grain boundary. On the top and bottom graphs we obtain a clear trend towards large mutual angles.

Energetics at lattice grain boundaries in small molecular systems

In the atomistic model of transport across grain boundaries in TIPS-P, we found that electrostatic interactions invariably lead to an energy barrier at the grain/grain interface. Here, we will show that the creation of an energy barrier is, however, by no means universal: notably, other interfacial energy profiles are conceivable, including trap and barrier/trap motifs.

As an abstraction of the complex atomistic description, we now employ a lattice model which (see also the Methods section) consists of probabilistically grown crystallites populated by quadrupolar particles with uniaxial symmetry. The molecular electrostatic layout is encoded in a single quadrupole component $Q_{20} = Q_{zz} < 0$ associated, for example, with the normal of the conjugated plane in compounds such as pentacene or the long axis of small molecules with an acceptor–donor–acceptor architecture. We also note that such a representation is (almost) as general as the quadrupole tensor in the eigenframe of a molecule has at best two non-zero components (Q_{20} and Q_{22c}).

Snapshots of the lattice systems are shown in Fig. 4a–d, where the yellow stripes in the top panels indicate the orientation of the domains. The four panels refer to different seed numbers (n = 2 to 16) included here to rule out grain-size effects. The electrostatic contribution $\Delta_{\mathrm{h}}^{(1)}$ to the site energy of holes is shown in the bottom panel, projected onto the xy-plane. First, it can be seen that the energy level within the domains is approximately constant. This intra-domain energy is determined by long-range interactions primarily *via* the out-of-plane component of the quadrupole tensor, which is identical for all grains, as they share the same orientation with respect to the thin-film normal. The energetics at the grain/grain interface, on the other hand, are exclusively determined by the short-range interaction of the excess (hole) charge with the polar end groups of the neighbouring grain. Due to the crystal packing and $Q_{20} < 0$ character of the polar sites, the energy profile across the interface is characterized by the concurrent appearance of a barrier and an adjacent trap (referred to as the

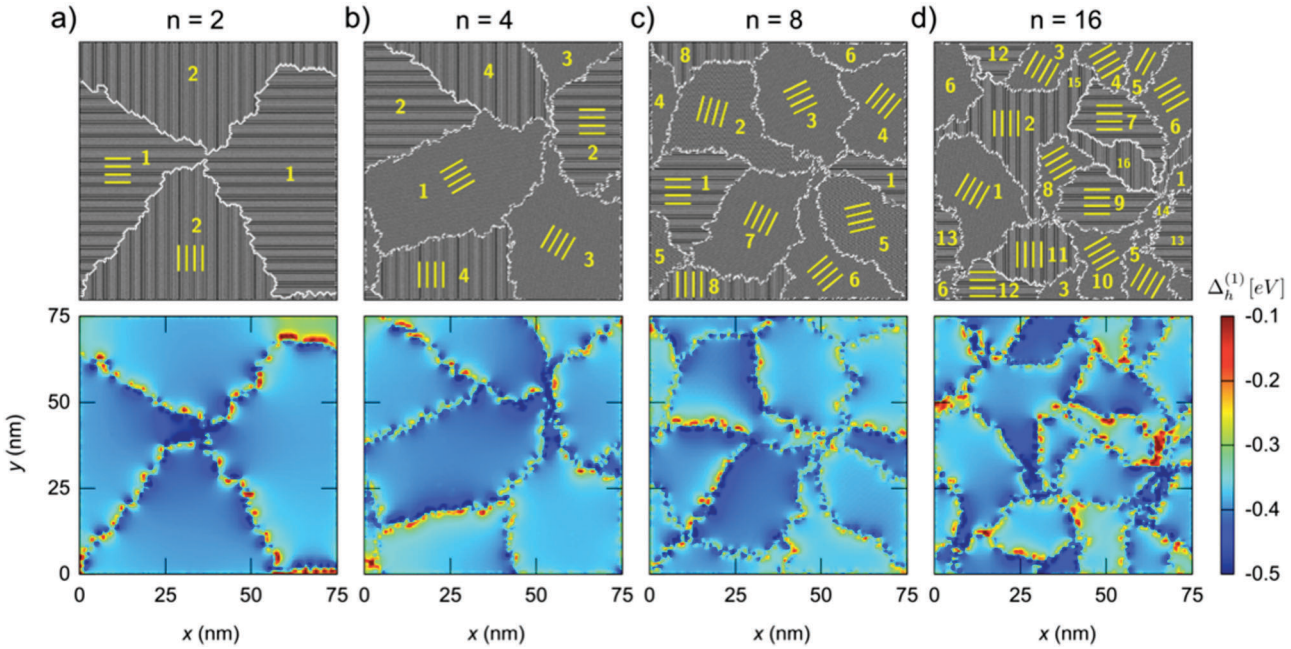

Fig. 4 Probabilistically grown Q_{20} face-centred square lattice grain boundaries with varying seed density from n = 2 (a) to n = 16 (d) seeds. The line blocks in the top panel indicate the orientation of the grains such that the line direction coincides with the local axis of the quadrupolar particles associated with the Q_{20} = −10 a.u. component. The bottom panel shows the electrostatic contribution to the energy landscape for holes projected onto the *xy*-plane.

barrier/trap motif), with an only slight dependence of the barrier height and well depth on the grain/grain angle. This barrier/trap motif should be contrasted with the pure-barrier motif found for holes in TIPS-P (see above).

It is important to note that for electrons the energy landscape is reversed ($\Delta_e^{(1)} = -\Delta_h^{(1)}$), as the formation of both barrier and barrier/trap structures is a result of the electrostatic (rather than polarization) contribution. This also implies that the high-energy states are not induced by a weaker dielectric stabilization due to interfacial voids. Changing from holes over to electrons, the barrier and barrier/trap therefore turn into a trap and trap/barrier motif, respectively. In the case of the lattice model from Fig. 4, charge-carrier migration across the boundary in the case of low carrier concentrations hence has to involve thermal activation independently of the type of the carrier. For TIPS-P, however, thermal activation is normally required only for electrons, which are likely to localize at an interfacial trap site. The grain/grain interface should therefore impact the effective activation energy for electron transport in TIPS-P, as probed by temperature-dependent mobility measurements. Holes, by contrast, can normally drift-diffuse through a gap in the barrier, since energetic disorder renders the boundary relatively porous, as demonstrated above for the case of large grain/grain interfaces. We tested the effect of the grain boundary on electron transport in our microscopic model of TIPS-P described above, and found that the effect of the grain boundary on electron transport is greater, by typically a factor of two, than the effect on hole transport.

Depending on molecular architecture and packing, all three interfacial energy motifs – barrier, trap, and barrier/trap (see Fig. 5) – are conceivable. For the barrier motif, migration across the grain boundary is limited by the time required to access a gap in the barrier, whereas for the well or barrier/well motif, the escape time from the trap serves as the controlling time scale for interdomain transport. The barrier motif is hence expected to exhibit the best transport properties. It is most likely to occur for low-energy packing modes (defined with respect to the carrier type in question, electrons or holes), as the disruption of the molecular arrangement caused by the grain boundary then necessarily implies the formation of higher-energy states.

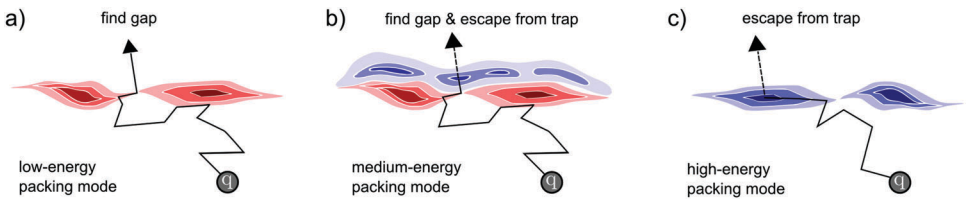

Fig. 5 Schematic of charge migration across a grain boundary for different interfacial energy profiles, including the (a) barrier, (b) barrier/trap and (c) trap motif.

Which packing mode (brickwork, herringbone, lamellar/columnar) presents a low-energy mode in turn depends on the molecular architecture. TIPS-P, for example, is characterized by a negative quadrupole component along the π-plane normal, next to a positive in-plane periphery composed of hydrogenated end groups. Pentacene has a similar quadrupolar structure. At the grain boundary, the bidirectional π–π arrangement is lost, with the result that the positive end groups of the neighbouring grain destabilize hole carriers and the energy of the structure is invariably raised for holes.

4 Conclusion

In conclusion, we have studied the impact of grain boundaries on charge transport in thin films of TIPS-P. We find that disruption of the crystalline packing at the grain boundaries leads to energetic barriers for hole transport (and potential wells for electrons) due to disruption of the low energy packing mode in the crystal. The impact is to slow down hole transport by a factor of $\approx 10^2$ relative to the crystalline film, with a minimal dependence on the inter-grain angle. The effect becomes stronger for limited contact areas due to the confinement of charge transport to high energy pathways. Thus, in order to explain strong mobility reductions due to grain boundaries, grain/grain contact areas must be small. This might be the case if the boundaries contain voids or are built from small, interconnected grains as proposed by Wong *et al.*[17] (see ESI,† Section C). The formation of energy barriers at interfaces without voids is, however, by no means universal: the energy level profile across grain/grain interfaces can exhibit barrier, barrier/trap and trap motifs depending on molecular architecture, packing and charge-carrier type. For low charge-carrier concentrations, low-site-energy packing modes are most desirable, as the distortion of the supramolecular structure at the grain boundary then creates energy barriers made permeable by energetic disorder, thus providing a mobility-maintaining pathway for intergranular transport. The transport model is based on a hopping picture which is justified here by the substantial energetic and configurational disorder at grain boundaries which mean that hopping events in these disordered regions will dominate the transport. In the case of a more ordered system, at lower temperature, it may be necessary to invoke more complex models that more accurately represent the delocalised nature of the charged states.

Acknowledgements

Florian Steiner would like to thank the Xerox Foundation/Xerox Research Centre of Canada (XRCC) and the DAAD for their financial support. Jenny Nelson thanks the UK Engineering and Physical Sciences Research Council (grant numbers EP/K029843/1, EP/K030671/1 and EP/M025020/1) for financial support and the Royal Society for a Wolfson Research Merit Award. This work was in part supported by the BMBF grants MEDOS (FKZ 03EK3503B), MESOMERIE (FKZ 13N10723), and InterPhase (FKZ 13N13661). The project has received funding from the NMP-20-2014 – ''Widening materials models'' program under Grant Agreement No. 646259 (MOSTOPHOS).

References

1 T. W. Kelley and C. D. Frisbie, *J. Phys. Chem. B*, 2001, **105**, 4538–4540.
2 G. Horowitz and M. Hajlaoui, *Synth. Met.*, 2001, **122**, 185–189.
3 V. Kalihari, E. Tadmor, G. Haugstad and C. D. Frisbie, *Adv. Mater.*, 2008, **20**, 4033–4039.
4 J. Rivnay, S. C. B. Mannsfeld, C. E. Miller, A. Salleo and M. F. Toney, *Chem. Rev.*, 2012, **112**, 5488–5519.
5 R. De Boer, T. Klapwijk and A. Morpurgo, *Appl. Phys. Lett.*, 2003, **83**, 4345–4347.
6 J. Soeda, T. Uemura, T. Okamoto, C. Mitsui, M. Yamagishi and J. Takeya, *Appl. Phys. Express*, 2013, **6**, 076503.
7 A. Facchetti, *Nat. Mater.*, 2013, **12**, 598–600.
8 Y. Diao, B. C. Tee, G. Giri, J. Xu, D. H. Kim, H. A. Becerril, R. M. Stoltenberg, T. H. Lee, G. Xue and S. C. Mannsfeld, *Nat. Mater.*, 2013, **12**, 665–671.
9 J. Chen, C. K. Tee, M. Shtein, J. Anthony and D. C. Martin, *J. Appl. Phys.*, 2008, **103**, 114513.
10 R. L. Headrick, S. Wo, F. Sansoz and J. E. Anthony, *Appl. Phys. Lett.*, 2008, **92**, 063302.
11 J. Rivnay, L. H. Jimison, J. E. Northrup, M. F. Toney, R. Noriega, S. Lu, T. J. Marks, A. Facchetti and A. Salleo, *Nat. Mater.*, 2009, **8**, 952–958.
12 X. Xu, Y. Yao, B. Shan, X. Gu, D. Liu, J. Liu, J. Xu, N. Zhao, W. Hu and Q. Miao, *Adv. Mater.*, 2016, **28**, 5276–5283.
13 J. Lee, S. Roth and Y. Park, *Appl. Phys. Lett.*, 2006, **88**, 252106.
14 O. Ostroverkhova, D. G. Cooke, F. A. Hegmann, R. R. Tykwinski, S. R. Parkin and J. E. Anthony, *Appl. Phys. Lett.*, 2006, **89**, 192113.
15 K. Puntambekar, J. Dong, G. Haugstad and C. D. Frisbie, *Adv. Funct. Mater.*, 2006, **16**, 879–884.
16 S. S. Lee, J. M. Mativetsky, M. A. Loth, J. E. Anthony and Y.-L. Loo, *ACS Nano*, 2012, **6**, 9879–9886.
17 C. Y. Wong, B. L. Cotts, H. Wu and N. S. Ginsberg, *Nat. Commun.*, 2015, **6**, 5946.
18 J. Y. Seto, *J. Appl. Phys.*, 1975, **46**, 5247–5254.
19 G. Baccarani, B. Ricco and G. Spadini, *J. Appl. Phys.*, 1978, **49**, 5565–5570.
20 J. Levinson, F. R. Shepherd, P. J. Scanlon, W. D. Westwood, G. Este and M. Rider, *J. Appl. Phys.*, 1982, **53**, 1193–1202.
21 G. Horowitz and M. E. Hajlaoui, *Adv. Mater.*, 2000, **12**, 1046–1050.
22 J. Cornil, S. Verlaak, N. Martinelli, A. Mityashin, Y. Olivier, T. Van Regemorter, G. Davino, L. Muccioli, C. Zannoni and F. Castet, *Acc. Chem. Res.*, 2012, **46**, 434–443.
23 G. D'Avino, S. Mothy, L. Muccioli, C. Zannoni, L. Wang, J. Cornil, D. Beljonne and F. Castet, *J. Phys. Chem. C*, 2013, **117**, 12981–12990.

24 C. Poelking, M. Tietze, C. Elschner, S. Olthof, D. Hertel, B. Baumeier, F. Würthner, K. Meerholz, K. Leo and D. Andrienko, *Nat. Mater.*, 2015, **14**, 434–439.
25 C. Poelking and D. Andrienko, *J. Am. Chem. Soc.*, 2015, **137**, 6320–6326.
26 J. W. Park, K. I. Lee, Y.-S. Choi, J.-H. Kim, D. Jeong, Y.-N. Kwon, J.-B. Park, H. Y. Ahn, J.-I. Park, H. S. Lee and J. Shin, *Phys. Chem. Chem. Phys.*, 2016, **18**, 21371–21380.
27 M. Mladenovic, N. Vukmirovic and I. Stankovic, *J. Phys. Chem. C*, 2013, **117**, 15741–15748.
28 H. Mathieu and H. Fanet, *Physique des semiconducteurs et des composants electroniques: Cours et exercices corriges*, DUNOD, 6th edn, 2009.
29 F. Steiner, S. Foster, A. Losquin, J. Labram, T. D. Anthopoulos, J. M. Frost and J. Nelson, *Mater. Horiz.*, 2015, **2**, 113–119.
30 J. Chen, D. C. Martin and J. Anthony, *J. Mater. Res.*, 2007, **22**, 1701–1709.
31 J. Wade, F. Steiner, D. Niedzialek, D. T. James, Y. Jung, D.-J. Yun, D. D. Bradley, J. Nelson and J.-S. Kim, *J. Mater. Chem. C*, 2014, **2**, 10110–10115.
32 J. E. Anthony, J. S. Brooks, D. L. Eaton and S. R. Parkin, *J. Am. Chem. Soc.*, 2001, **123**, 9482–9483.
33 W. L. Jorgensen, D. S. Maxwell and J. Tirado-Rives, *J. Am. Chem. Soc.*, 1996, **118**, 11225–11236.
34 A. A. Y. Guilbert, J. M. Frost, T. Agostinelli, E. Pires, S. Lilliu, J. E. Macdonald and J. Nelson, *Chem. Mater.*, 2014, **26**, 1226–1233.
35 V. Ruehle, C. Junghans, A. Lukyanov, K. Kremer and D. Andrienko, *J. Chem. Theory Comput.*, 2009, **5**, 3211–3223.
36 J. J. Kwiatkowski, J. M. Frost and J. Nelson, *Nano Lett.*, 2009, **9**, 1085–1090.
37 J.-F. Chang, T. Sakanoue, Y. Olivier, T. Uemura, M.-B. Dufourg-Madec, S. G. Yeates, J. Cornil, J. Takeya, A. Troisi and H. Sirringhaus, *Phys. Rev. Lett.*, 2011, **107**, 066601.
38 R. A. Marcus, *J. Chem. Phys.*, 1956, **24**, 966.
39 J. Nelson, J. J. Kwiatkowski, J. Kirkpatrick and J. M. Frost, *Acc. Chem. Res.*, 2009, **42**, 1768–1778.
40 T. Sakanoue and H. Sirringhaus, *Nat. Mater.*, 2010, **9**, 736–740.
41 J. Kirkpatrick, *Int. J. Quantum Chem.*, 2008, **108**, 51–56.
42 J.-L. Bredas, D. Beljonne, V. Coropceanu and J. Cornil, *Chem. Rev.*, 2004, **104**, 4971–5004.
43 V. Rühle, A. Lukyanov, F. May, M. Schrader, T. Vehoff, J. Kirkpatrick, B. Baumeier and D. Andrienko, *J. Chem. Theory Comput.*, 2011, **7**, 3335–3345.
44 B. Baumeier, J. Kirkpatrick and D. Andrienko, *Phys. Chem. Chem. Phys.*, 2010, **12**, 11103–11113.
45 A. Kubas, F. Hoffman, A. Heck, H. Oberhofer, M. Elstner and J. Blumberger, *J. Chem. Phys.*, 2014, **140**, 104105.
46 J. Spencer, L. Scalfi, A. Carof and J. Blumberger, *Faraday Discuss.*, 2016, **195**, 215–236.

